

AD-A113 013

DCW INDUSTRIES INC. STUDIO CITY CA

F/O 20/4

NUMERICAL ALGORITHM FOR RAPID INTEGRATION OF TURBULENCE-MODEL E-ETC(U)

FEB 82 D C WILCOX

F49620-78-C-0024

UNCLASSIFIED

DCW-R-21-04

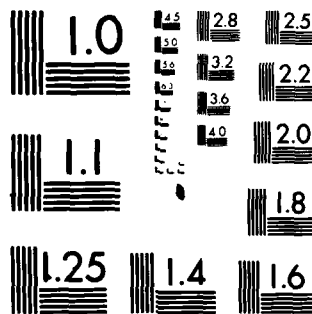
AFOSR-TR-82-0213

NL

10-1
2-10-82

DCW INDUSTRIES
10-1

END
DATE
FILMED
4-82
DTIC



MICROCOPY RESOLUTION TEST CHART
NATIONAL BUREAU OF STANDARDS 1963-A

Final
12

AD A11 3013

DCW INDUSTRIES

DTIC FILE COPY

DTIC
ELECTE
S APR 6 1982 D
D

4367 TROOST AVENUE, STUDIO CITY, CALIFORNIA 91604

82 04 06 031

F49620-78-C-0024

Approved for public release;
distribution unlimited.

DCW-R-21-04

NUMERICAL ALGORITHM
FOR RAPID INTEGRATION OF
TURBULENCE-MODEL EQUATIONS
ON ELLIPTIC REGIONS

by

David C. Wilcox

FINAL SCIENTIFIC REPORT

February 1982

Prepared for

AIR FORCE OFFICE OF SCIENTIFIC RESEARCH
Air Force Systems Command
Bolling AFB, Washington, D. C.

Under Contract F49620-78-C-0024

AIR FORCE OFFICE OF SCIENTIFIC RESEARCH (AFSC)
NOTED
This report is for the use of the Air Force
applicable to the Air Force
Distributed to the Air Force
MATT
Chief, Information Division

DCW Industries, Inc.

4367 Troost Avenue

Studio City, California 91604

213/769-7571 or 213/790-3844



Accession For	
NTIS GRA&I	<input checked="" type="checkbox"/>
DTIC TAB	<input type="checkbox"/>
Unannounced	<input type="checkbox"/>
Justification	
By	
Distribution/	
Availability Codes	
Dist	Avail and/or Special
<input type="checkbox"/>	

UNCLASSIFIED

SECURITY CLASSIFICATION OF THIS PAGE (When Data Entered)

REPORT DOCUMENTATION PAGE		READ INSTRUCTIONS BEFORE COMPLETING FORM
1. REPORT NUMBER AFOCR-TR- 82 0213	2. GOVT ACCESSION NO AD-A113 013	3. RECIPIENT'S CATALOG NUMBER
4. TITLE (and Subtitle) NUMERICAL ALGORITHM FOR RAPID INTEGRATION OF TURBULENCE-MODEL EQUATIONS ON ELLIPTIC REGIONS		5. TYPE OF REPORT & PERIOD COVERED FINAL 1 March 1978-31 Dec1981
		6. PERFORMING ORG. REPORT NUMBER
7. AUTHOR(s) David C. Wilcox		8. CONTRACT OR GRANT NUMBER(s) F49620-78-C-0024
9. PERFORMING ORGANIZATION NAME AND ADDRESS DCW INDUSTRIES 4367 Troost Avenue Studio City, California 91604		10. PROGRAM ELEMENT, PROJECT, TASK AREA & WORK UNIT NUMBERS 66102F 2307/A4
11. CONTROLLING OFFICE NAME AND ADDRESS Air Force Office of Scientific Research/NA Bolling Air Force Base, D C 20332		12. REPORT DATE February 1982
		13. NUMBER OF PAGES 26
14. MONITORING AGENCY NAME & ADDRESS (if different from Controlling Office)		15. SECURITY CLASS. (of this report) UNCLASSIFIED
		15a. DECLASSIFICATION/DOWNGRADING SCHEDULE
16. DISTRIBUTION STATEMENT (of this Report) Approved for public release; distribution unlimited		
17. DISTRIBUTION STATEMENT (of the abstract entered in Block 20, if different from Report)		
18. SUPPLEMENTARY NOTES		
19. KEY WORDS (Continue on reverse side if necessary and identify by block number) TURBULENCE MODEL NUMERICS MICROPROCESSORS		
20. ABSTRACT (Continue on reverse side if necessary and identify by block number) A numerical algorithm suitable for rapid numerical solution of advanced turbulence-model equations on elliptic regions has been devised. The algorithm is particularly useful for obtaining accu- rate solutions when (a) one of the dependent variables is singular approaching a solid boundary, and (b) the number of mesh points available to resolve the flowfield is small. The new algorithm is used in conjunction with the MacCormack semi-implicit scheme for solving the time-averaged Navier-Stokes equations to obtain		

DD FORM 1 JAN 73 1473

EDITION OF 1 NOV 65 IS OBSOLETE

UNCLASSIFIED

V

SECURITY CLASSIFICATION OF THIS PAGE (When Data Entered)

UNCLASSIFIED

SECURITY CLASSIFICATION OF THIS PAGE(When Data Entered)

solutions for a laminar Mach 2 boundary layer and for a turbulent Mach 3 boundary layer. In both cases, numerical accuracy is shown to be excellent for meshes having less than 20 points normal to the surface. As a corollary result of this study we have shown that, using the new algorithm and the MacCormack scheme, time-averaged Navier-Stokes solutions are now feasible using a microcomputer. *+*

UNCLASSIFIED

v1 SECURITY CLASSIFICATION OF THIS PAGE(When Data Entered)

ABSTRACT

A numerical algorithm suitable for rapid numerical solution of advanced turbulence-model equations on elliptic regions has been devised. The algorithm is particularly useful for obtaining accurate solutions when (a) one of the dependent variables is singular approaching a solid boundary and (b) the number of mesh points available to resolve the flowfield is small. The new algorithm is used in conjunction with the MacCormack semi-implicit scheme for solving the time-averaged Navier-Stokes equations to obtain solutions for a laminar Mach 2 boundary layer and for a turbulent Mach 3 boundary layer. In both cases, numerical accuracy is shown to be excellent for meshes having less than 20 points normal to the surface. As a corollary result of this study we have shown that, using the new algorithm and the MacCormack scheme, time-averaged Navier-Stokes solutions are now feasible using a micro-computer.

FOREWORD

This report presents a summary of research performed in Contract F49620-78-C-0024 during the period March 1, 1978 through December 31, 1981. This research was sponsored by the Air Force Office of Research (AFSC), United States Air Force. The Air Force program monitor was Dr. James Wilson.

Study participants were Dr. David C. Wilcox, principal investigator, and Barbara A. Wilcox, contract administrator and data processing support. Manuscript preparation was done by Kinley A. Wilcox.

1. INTRODUCTION

During the course of this research project (and also in a numerical study funded by the NASA Ames Research Center¹) we have found that conventional time-marching numerical methods encounter serious difficulty in solving advanced turbulence-model equations. This difficulty has impeded our progress toward the ultimate goal of this research project, viz, development of a numerical method for simulating viscous flow in axial turbomachines. Thus, during the past year our efforts have focused on the cause of and the resolution of this numerical difficulty.

Prior to this study we found that numerically-accurate steady-flow solutions generally cannot be obtained for complex turbulent flows under the following conditions:

1. an advanced turbulence model with additional dependent variables, one of which usually is singular near solid boundaries, is used;
2. a severely limited number of points are available to define the computational mesh for the region of interest;
3. the equations are integrated through the viscous sublayer.

For our axial turbomachine applications, all three of the conditions cited above exist. Firstly, we are using the Wilcox-Rubesin² two-equation model of turbulence which involves a dependent variable that becomes singular upon approach to a solid boundary. Secondly, the flowfield in axial turbomachines inherently is three dimensional and, because computers have limited memory, we anticipate having no more than 15 mesh points normal to a blade surface contained within boundary layers. Finally, because we feel that physically meaningful solutions on separation regions require integration through the viscous sublayer, and because we want our method to treat the separated case, our applications include integration through the viscous sublayers.

Prior to this study, Wilcox¹ identified two possible sources of inaccuracy and/or numerical instability which might plague conventional time-marching methods. He demonstrated that the singular

behavior of the turbulent dissipation rate near a solid boundary cannot be accurately computed with central differences. In an unsuccessful attempt at analytically removing the singularity with a straightforward change of dependent variables, improved numerical accuracy was accompanied by slowly growing numerical oscillations elsewhere in the flowfield. Wilcox speculated that the source of these oscillations was the numerical-algorithm-induced (and physically unrealistic) coupling between the turbulence production processes and the unsteady rate of change of the turbulence.

In this study, we have devised a numerical algorithm which lacks the shortcomings of conventional, central-differences-oriented, time-marching methods when applied to turbulence-model equations. The method's accuracy and stability have been assessed in two viscous-flow computations (both performed on a microcomputer), neither of which can be done accurately with a conventional time-marching method unless far more mesh points are used.

Section 2 presents the equations of motion and pinpoints the root causes of the numerical inaccuracy and instabilities encountered in our attempts to compute viscous flowfields. In Section 3, a new algorithm is devised to circumvent these difficulties; application to a simplified turbulence-model equation demonstrates a dramatic improvement in numerical accuracy over conventional algorithms. Section 4 presents results of two time-averaged Navier-Stokes computations, one for a laminar Mach 2 boundary layer and the other for a turbulent Mach 3 boundary layer. In both cases, results are (correctly) obtained which appear unobtainable with a conventional time-marching method. The concluding section summarizes results and conclusions.

The Bibliography and Contract Overview sections summarize publications and highlights of the overall research effort in this Contract.

2. EQUATIONS OF MOTION AND ASSOCIATED NUMERICAL DIFFICULTIES

This section first presents the basic equations of motion used in this project. A summary of the numerical difficulties encountered in trying to solve these equations follows, including a discussion of truncation error and numerical stability.

2.1 EQUATIONS OF MOTION

The equations of motion used in all of our computations are those devised by Wilcox and Rubesin². The model assumes the Reynolds stress tensor, τ_{ij} , is proportional to the mean strain-rate tensor, S_{ij} , as follows.

$$\tau_{ij} = 2\rho\epsilon \left(S_{ij} - \frac{1}{3} \frac{\partial u_k}{\partial x_k} \delta_{ij} \right) - \frac{2}{3} \rho e \delta_{ij} \quad (1)$$

In equation (1), ρ is mass density, ϵ is the eddy diffusivity, u_i is the velocity vector, x_j is position vector, δ_{ij} is the Kronecker delta, and e is the turbulent mixing energy. All quantities are understood to be mass averaged in the sense introduced by Favre³. The mean conservation equations are:

$$\frac{\partial \rho}{\partial t} + \frac{\partial}{\partial x_j} (\rho u_j) = 0 \quad (2)$$

$$\frac{\partial}{\partial t} (\rho u_i) + \frac{\partial}{\partial x_j} (\rho u_j u_i) = \frac{\partial}{\partial x_j} \left\{ 2\mu \left(S_{ij} - \frac{1}{3} \frac{\partial u_k}{\partial x_k} \delta_{ij} \right) + \tau_{ij} - p \delta_{ij} \right\} \quad (3)$$

$$\frac{\partial E}{\partial t} + \frac{\partial}{\partial x_j} (u_j E) = \frac{\partial}{\partial x_j} \left\{ u_i (\tau_{ij} - p \delta_{ij}) + k \frac{\partial T}{\partial x_j} + (\mu + \sigma^* \rho \epsilon) \frac{\partial e}{\partial x_j} \right\} \quad (4)$$

where t denotes time, p is static pressure, μ is molecular viscosity, k is the sum of molecular and turbulent heat diffusivities, T is static temperature, σ^* is a turbulent closure coefficient which will

be discussed below, and E is the total energy defined by the following relation.

$$E = C_v T + \frac{1}{2} \rho u_1 u_1 + \rho e \quad (5)$$

where C_v is specific heat coefficient at constant volume.

In addition to Equations (1-5), the Wilcox-Rubesin model introduces two additional "rate equations" for the turbulent mixing energy, e , and the turbulent dissipation rate, ω , from which the eddy diffusivity is computed. The equations are as follows.

$$\frac{\partial}{\partial t} (\rho e) + \frac{\partial}{\partial x_j} (\rho u_j e) = \tau_{1j} \frac{\partial u_1}{\partial x_j} - \beta^* \rho \omega e + \frac{\partial}{\partial x_j} \left\{ (\mu + \sigma^* \rho \epsilon) \frac{\partial e}{\partial x_j} \right\} \quad (6)$$

$$\begin{aligned} \frac{\partial}{\partial t} (\rho \omega^2) + \frac{\partial}{\partial x_j} (\rho u_j \omega^2) = & \gamma_e^2 \tau_{1j} \frac{\partial u_1}{\partial x_j} - \left\{ \beta + 2\sigma \left(\frac{\partial \ell}{\partial x_k} \right)^2 \right\} \rho \omega^3 \\ & + \frac{\partial}{\partial x_j} \left\{ (\mu + \sigma \rho \epsilon) \frac{\partial \omega^2}{\partial x_j} \right\} \end{aligned} \quad (7)$$

The eddy diffusivity, ϵ , and the turbulent length scale, ℓ , are obtained from e and ω according to:

$$\epsilon = \gamma^* e / \omega \quad (8)$$

$$\ell = e^{1/2} / \omega \quad (9)$$

Finally, we introduce a turbulent Prandtl number, Pr_T , and express the turbulent heat flux vector as being proportional to the mean temperature gradient so that the thermal conductivity, k , in Equation (5) becomes:

$$k = \left\{ \mu / Pr_L + \rho \epsilon / Pr_T \right\} C_v \quad (10)$$

Where Pr_L is laminar Prandtl number. Six closure coefficients appear in Equations (6-8), viz, β , β^* , γ , γ^* , σ , and σ^* . The values of these closure coefficients have been established from widely observed properties of turbulent flows. Their values are:

$$\left. \begin{aligned} \beta &= 3/20 & \beta^* &= 9/100 \\ \sigma &= 1/2 & \sigma^* &= 1/2 \\ \gamma^* &= \{ 1 - (1 - \lambda^2) \exp(-Re_T) \} \\ \gamma \gamma^* &= 10/9 \{ 1 - (1 - \lambda^2) \exp(-Re_T/2) \} \\ \lambda &= 1/11 \end{aligned} \right\} \quad (11)$$

and the quantity Re_T is the Reynolds number of the turbulence defined in terms of the dependent variables by:

$$Re_T = \rho e / (\omega \mu) \quad (12)$$

Before proceeding to a discussion of boundary conditions in the next subsection, a key point about the equations of motion is worthy of note. In the mean-energy equation (4), note that the last term on the right-hand side generally is omitted by turbulence modelers. The origin of this term is obvious when the time-averaged equation for total energy, E , as defined in Equation (5) is derived. If this term is omitted, there is no guarantee that total energy, E , will be conserved in the flowfield, even when $e \ll C_V T$. This is true because its omission can give rise to nonphysical numerical oscillations whose energy source is unrelated to the physical energy of the flowfield.

2.2 BOUNDARY CONDITIONS

As noted in the Introduction, in our computation of the flowfields of interest, we integrate the equations of motion through the viscous sublayer. Thus, we must specify boundary conditions for the various dependent variables appropriate to a solid boundary. Denoting distance normal to the surface by y , we impose the no-slip velocity boundary condition at $y=0$. Additionally, for all compressible applications considered in this study, the surface is adiabatic. Thus, for the mean-flow quantities we have:

$$\left. \begin{array}{l} u_i = 0 \\ \partial T / \partial y = 0 \end{array} \right\} \quad \text{at} \quad y = 0 \quad (13)$$

Turning now to the turbulence properties, an additional consequence of the no-slip boundary condition is that the turbulent mixing energy (which is proportional to the square of fluctuating velocity components) vanishes at a solid boundary. Also, as noted by Wilcox and Rubesin², the turbulent dissipation rate approaches a known analytical form in the sublayer. For a perfectly smooth surface we have:

$$e = 0 \quad \text{at} \quad y = 0 \quad (14)$$

$$\omega \rightarrow \frac{20v_w}{\beta y^2} \quad \text{as} \quad y \rightarrow 0 \quad (15)$$

where subscript w denotes surface value.

Equation (15) illustrates a key point about the turbulence-model equations which is worthy of note. Remembering that the characteristic length scale of the turbulence, ℓ , is inversely proportional to ω approaching a solid boundary implies that ℓ becomes very small. This is consistent with the physics of turbulence which finds the constraint of a solid boundary admitting only the smallest eddies. Thus, even with the great advantages attending the use of long-time averaging (compared to, say, a large-eddy simulation), we still must deal with the problem of resolving very small eddies in a finite-difference computation. This "conservation of difficulty" stands at the center of the numerical woes attending solution of the turbulence-model equations.

Finally, as will be illustrated in the next subsection, the dissipation rate is singular (although less strongly than y^{-2}) far above the viscous sublayer. Thus, the numerical difficulties we have encountered are not caused entirely by our treatment of the sublayer. Rather, all advanced turbulence models share the same unpleasant (from a numerical standpoint) behavior.

2.3 TRUNCATION ERRORS

Virtually all finite-difference numerical schemes used for solving the time-averaged Navier Stokes equations employ central differences. Usually, such schemes are of second-order accuracy in both time and space. In our work, for example, we have used variants of the MacCormack time-splitting method⁴⁻⁶ which uses second-order accurate, central differences. Even for relatively crude meshes, such a scheme is satisfactory when the various dependent variables are analytic throughout the flowfield. However, when one of the dependent variables is nonanalytic, such as ω , truncation errors can become very large.

For example, Figure 1 compares the computed near-surface behavior of ω with the theoretical limiting form given in Equation (15). The profile

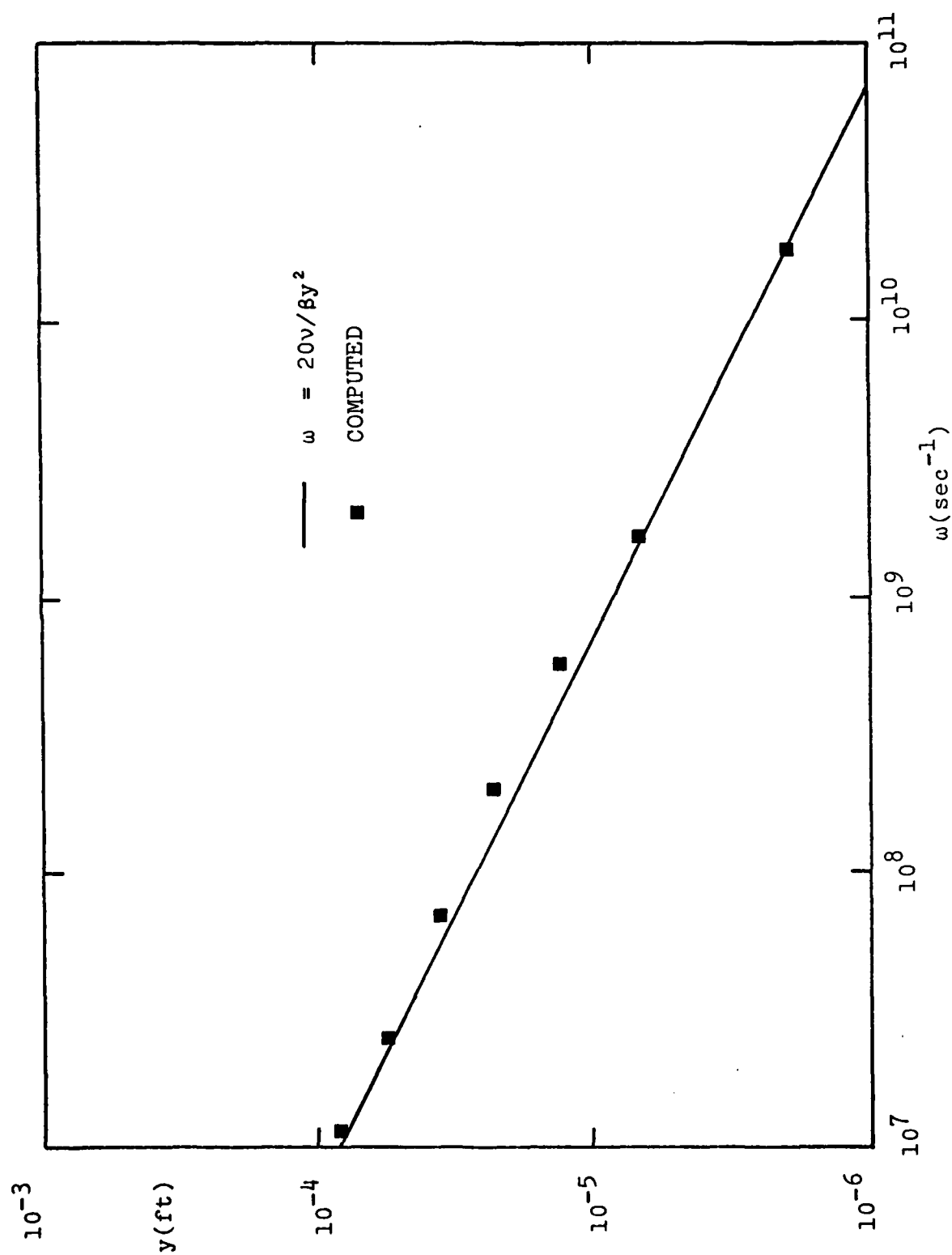


Figure 1. Comparison of computed near-wall dissipation-rate profile with the asymptotic limiting behavior; Mach 3 flat-plate boundary layer.

shown is for a Mach 3, adiabatic-wall boundary layer. Long experience with the model equations has shown that, for a wide range of flows both incompressible and compressible, very close to the surface ($y^+ = u_\tau y / \nu_w < 4$) Equation (15) is valid. As shown, the computed values of ω are 20% - 30% higher than the theoretical values. Our experience with these model equations has shown that this large an error in ω has a large effect on predicted flow properties throughout the boundary layer.

The reason such truncation errors persist far above the sublayer becomes obvious upon inspection of the limiting form of ω in the logarithmic (law-of-the-wall) region. As shown by Saffman and Wilcox⁷, approaching the sublayer from above we have

$$\omega \rightarrow \frac{u_\tau \sqrt{\rho_w / \rho}}{\sqrt{\beta^*} \kappa y} \quad \text{as} \quad y^+ \rightarrow 0 \quad (16)$$

where $\kappa = 0.41$ is Karman's constant and u_τ is friction velocity. Thus, even far above the viscous sublayer ω is nonanalytic and the use of central differences is attended by nontrivial truncation errors.

The source of the numerical inaccuracy becomes obvious if we consider the magnitude of the errors introduced when using central differences to compute derivatives of ω^2 close to the surface. Because we solve the equations of motion in conservation form, the finite-difference formulation actually computes $\rho \omega^2$ which (ignoring density for simplicity) exhibits strongly singular behavior, viz,

$$\omega^2 \sim y^{-4} \quad \text{as} \quad y \rightarrow 0 \quad (17)$$

It is easy to show if we use the exact values of ω^2 at two adjacent mesh points y_j and y_{j+1} , central differences yield:

$$\left(\frac{\partial \omega^2}{\partial y} \right)_{j+\frac{1}{2}} \doteq \left(\frac{\partial \omega^2}{\partial y} \right)_{\text{exact}} \cdot \frac{(1+\epsilon^2)}{(1-\epsilon^2)^4} \quad (18)$$

where

$$\epsilon \equiv \frac{y_{j+1} - y_j}{y_{j+1} + y_j} \quad (19)$$

Because of the fine resolution close to the surface (for the point nearest the surface the computation of Figure 1 has $y^+ \approx \frac{1}{4}$) the smallest value of ϵ for the mesh used is 1/5. Using this value for ϵ in Equation (18) yields

$$\left(\frac{\partial \omega^2}{\partial y}\right)_{j+\frac{1}{2}} = 1.27 \left(\frac{\partial \omega^2}{\partial y}\right)_{\text{exact}} \quad (20)$$

Thus, using conventional central differences yields more than a 25% error when computing derivatives.

In order to illustrate the point that the truncation errors persist far beyond the sublayer, Figure 2 shows results of a computed ω profile obtained from solution of a simplified version of Equation (7). Specifically, we have dropped all but the dissipation and molecular diffusion terms so that, for incompressible flow, the equation simplifies to

$$\nu \frac{d^2 \omega^2}{dy^2} = \beta \omega^3 \quad (21)$$

the exact solution of which is

$$\omega = \frac{20\nu}{\beta y^2} \quad (22)$$

The figure shows results of two computations both of which use a mesh similar to that of the Navier-Stokes computation discussed above. That is, mesh points normal to the surface are spaced in a geometric progression with progression ratio $k = 1.25$. In the first computation, the value of ω at the mesh point nearest the surface is obtained from Equation (22). As shown, the local error close to the surface is in excess of 50%. In the second computation, Equation (22) is used to prescribe the value of ω for the 10 mesh points nearest the surface (a procedure used in most of our past computations provided mesh point number 10 lies below $y^+ = 4$). While the local error is reduced significantly near the surface, there is little improvement in accuracy farther from $y = 0$.

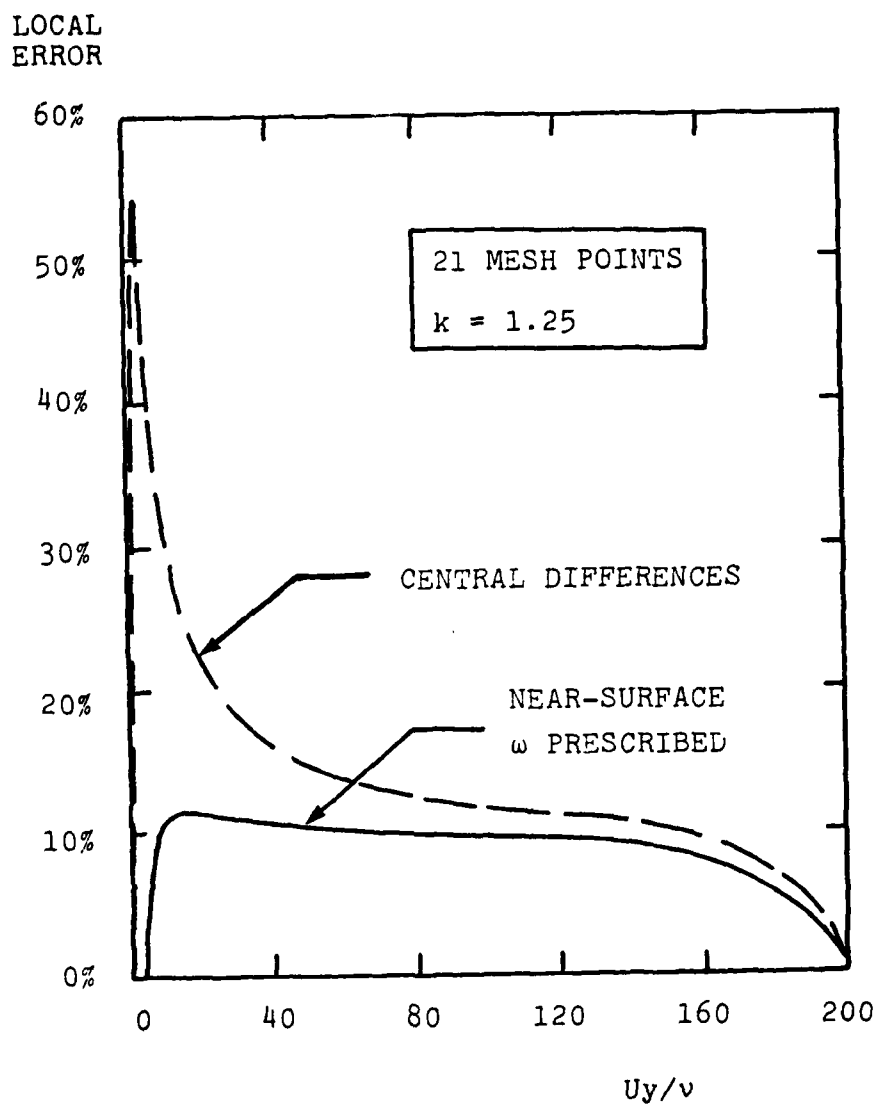


Figure 2. Effect of prescribing near-surface singularity analytically.

2.4 STABILITY CONSIDERATIONS

A second, less obvious, numerical difficulty becomes evident upon considering the stability of a given numerical scheme when applied to the model equations. A simplified version of the equations for e and ω^2 which illustrates potential problems is as follows.

$$\frac{\partial e}{\partial t} + u \frac{\partial e}{\partial x} = P e + \nu \frac{\partial^2 e}{\partial x^2} \quad (23)$$

In Equation (23), P denotes net production, viz, production minus dissipation. In the case where P is constant, it is easy to show that even for a typical implicit second-order accurate time-marching scheme, positive P leads to unconditional instability¹ in the classical sense. This is unsurprising however as solutions to Equation (23), subject to certain initial and boundary conditions, grow exponentially in time. Thus, even though local errors might be small compared to the solution itself, they will also grow exponentially. A numerical analysis of Equation (23) performed in this study verified this instability when P is positive.

A key shortcoming of the model equation (23) is the independence of e from the mean kinetic energy. In any physical flow, there will not be an infinite source of energy as implied in Equation (23). Rather, the coefficient P will increase at the expense of the mean kinetic energy and u will decrease. To simulate this situation we studied a model in which we have

$$P = p u^2 - \beta \omega \quad (24)$$

$$\frac{1}{2} u^2 + e = \text{constant} \quad (25)$$

where p is a constant and an equation similar to Equation (23) is written for ω^2 . Using MacCormack's explicit scheme⁴, this system displays no numerical instability for Courant numbers less than one. Thus, as noted in Subsection 2.1, if we are not careful enough in writing our turbulence model equations to insure conservation of total energy, unusual numerical instability may arise.

However, it is still possible for the production term to cause large numerical excursions from the steady state, especially if the initial flowfield is quite different from the long-time solution. In the ω equation, for example, very close to the surface we should find a balance between dissipation and molecular diffusion. By contrast we have often observed a strong (nonphysical) coupling between the unsteady and the dissipation terms which causes ω^2 to become negative. Hence, the presence of the source terms can present numerical problems quite unlike those encountered with conventional conservation equations.

3. A NEW ALGORITHM

In this section we present a new algorithm which simultaneously eliminates truncation errors and effectively removes nonphysical coupling between source and unsteady terms. First we motivate and present the algorithm; then we apply it to Equation (21).

3.1 MOTIVATION

In a previous study, Wilcox¹ tried removing the near-wall singularity analytically by making the straightforward change of variables:

$$\omega^2 = \psi/y^4 \quad (26)$$

The function ψ is analytic as $y \rightarrow 0$ and presumed a more appropriate quantity to compute. However, using the MacCormack hybrid explicit-implicit method⁵ Wilcox simultaneously (a) improved near-wall accuracy and (b) introduced large (bounded) numerical oscillations. While this change of variables eliminates truncation errors, it apparently aggravates numerical stability via attending alteration of the source terms.

To provide motivation for the new algorithm which will be presented in the following Subsection, it is instructive to consider the limiting form of the ω equation upon approaching $y = 0$. It is easy to show that the equation has the following form for a constant-pressure boundary layer:

$$\frac{\partial^2 \omega^2}{\partial y^2} + \frac{q}{y} \frac{\partial \omega^2}{\partial y} - \frac{p}{y^2} \omega^2 = F \quad (27)$$

where precise details of the coefficients F , p and q are unimportant (see Equations 34-35 below). Of greatest importance is their behavior close to the surface where we find:

Viscous Sublayer ($y^+ < 10$)

$$\left. \begin{array}{l} F \rightarrow 0 \\ q \rightarrow 0 \\ p \rightarrow 20 \\ y^4 \omega^2 \rightarrow \text{constant} \end{array} \right\} \text{ as } y \rightarrow 0, y^+ < 10 \quad (28)$$

Wall Layer ($10 < y^+ < 100$)

$$\left. \begin{array}{l} F \rightarrow 0 \\ q \rightarrow 1 \\ p \rightarrow 4 \\ y^2 \omega^2 \rightarrow \text{constant} \end{array} \right\} \text{ as } y \rightarrow 0, 10 < y^+ < 100 \quad (29)$$

Inspection of Equations (28) and (29) shows that the singularity changes its strength across the sublayer/wall-layer interface. It further suggests that a more-appropriate transformation might reflect this fact.

3.2 THE ALGORITHM

The observations in the preceding Subsection suggest the following change of variables:

$$\omega^2 = \psi y^\chi \quad (30)$$

where χ is assumed to be a function of p and q and also of time, t . Substituting Equation (30) into Equation (7) yields

$$\frac{\partial}{\partial t}(\rho\psi) + \frac{\partial}{\partial x_j}(\rho u_j \psi) = \frac{2\chi(\mu + \sigma\rho\varepsilon)}{y} \frac{\partial\psi}{\partial y} + \frac{\partial}{\partial x_j} \left\{ (\mu + \sigma\rho\varepsilon) \frac{\partial\psi}{\partial x_j} \right\} \quad (31)$$

$$\left(\frac{\rho y^2 \log y}{\mu + \sigma\rho\varepsilon} \right) \frac{\partial\chi}{\partial t} = \chi^2 + \left\{ \frac{y \left\{ \frac{\partial}{\partial y} (\mu + \sigma\rho\varepsilon) - \rho v \right\}}{\mu + \sigma\rho\varepsilon} - 1 \right\} \chi + \frac{y^2 S}{\mu + \sigma\rho\varepsilon} \quad (32)$$

where

$$S = \gamma \frac{\tau_{11}}{e} \frac{\partial u_1}{\partial x_j} - \left\{ \beta + 2\sigma \left(\frac{\partial \ell}{\partial x_k} \right)^2 \right\} \rho \omega \quad (33)$$

There are three key points about the transformed equations worthy of note. First, while Equation (31) contains a nonconservation-like term, viz, the term proportional to $\partial\psi/\partial y$, the term shouldn't destroy numerical stability. The new term will behave more like an extra convective flux and should be far less troublesome provided it is differenced in a manner consistent with that used for the standard convective terms.

Second, the coefficients in the equation for χ are directly related

to the p and q appearing in Equation (27). In fact, we have

$$q = \frac{y \left\{ \frac{\partial}{\partial y} (\mu + \sigma \rho \epsilon) - \rho v \right\}}{\mu + \sigma \rho \epsilon} \quad (34)$$

$$p = - \frac{y^2 S}{\mu + \sigma \rho \epsilon} \quad (35)$$

Hence, in the steady state ($\partial \chi / \partial t = 0$) we have

$$\chi^2 + (q - 1)\chi - p = 0 \quad (36)$$

so that

$$\chi = \frac{1}{2}(1 - q) - \frac{1}{2}\sqrt{(1 - q)^2 + 4p} \quad (37)$$

where we have selected the root of Equation (36) which yields negative χ . Substituting the values of p and q from Equations (28-29) into Equation (37) shows that

$$\chi = \begin{cases} -4, & \text{in the sublayer} \\ -2, & \text{in the wall layer} \end{cases} \quad (38)$$

Thus, the transformation captures the proper nature of the singularity in both near-wall regions.

The final key point is that we have a method which requires no specific alteration of the particular numerical method used. Central differences should be satisfactory for computing ψ as it is an analytic function as $y \rightarrow 0$.

In summary, the change of dependent variables proposed in Equation (30) has the following three desirable features:

1. It replaces the $P\omega^2$ type source term with a more familiar convective-type term;
2. It reflects the varying strength of the ω^2 singularity in the near-wall region of a boundary layer;
3. It places no unusual constraint on the type of numerical algorithm used.

In principal, this transformation has very desirable properties. To provide a definitive numerical accuracy test, the next Subsection shows results of its application to Equation (21) for which the exact solution is known, i.e., Equation (22).

3.3 APPLICATION WITH A SIMPLIFIED MODEL

As our first application of the new algorithm, we consider the limiting near-wall form of the equation for ω , viz, Equation (21). This equation provides a definitive accuracy check as the exact solution is known and is given in Equation (22). The new MacCormack⁶ implicit method is used so that we introduce an unsteady term to Equation (21) and seek the long-time solution. Thus, the actual equation being solved is

$$\frac{\partial \omega^2}{\partial t} = \nu \frac{\partial^2 \omega^2}{\partial y^2} - \beta \omega^3 \quad (39)$$

Introducing the transformation defined in Equation (30) leads to the following equations for ψ and χ :

$$\frac{\partial \psi}{\partial t} = \nu \frac{\partial^2 \psi}{\partial y^2} + \frac{2\chi\nu}{y} \frac{\partial \psi}{\partial y} \quad (40)$$

$$\left(\frac{y^2 \log y}{\nu}\right) \frac{\partial \chi}{\partial t} = \chi^2 - \chi - \beta y^2 \omega / \nu \quad (41)$$

where ω is understood to be computed from ψ and χ according to Equation (30). In the steady state, the exact solution to Equations (40) and (41) is

$$\psi = 20\nu/\beta \quad (42)$$

$$\chi = -4 \quad (43)$$

These equations have been solved using a grid with equally spaced mesh points. Such a grid which would yield even larger truncation errors than shown in Figure 2 if we solved Equation (39) without the transformation to ψ and χ . The grid was also constructed to insure that the nondimensional y coordinate, viz,

$$\bar{y} = Uy/\nu \quad (44)$$

where U is a characteristic velocity, will always be greater than unity. Early numerical experimentation showed that Equation (41) is more easily solved if the logy term on the left-hand side retains the same sign throughout the mesh.

The initial profiles for ψ and χ were varied about the exact steady-state values given in Equations (42) and (43).

In all computations, no more than 50 timesteps were required to reach steady-state. Regardless of the initial conditions, the solution converged to within six significant figures of the exact solution. Thus, at least for this simplified test case, the transformation defined in Equation (30) yields greatly improved numerical accuracy.

Because the exact solution to Equations (40-41) is $\psi = \text{constant}$ and $\chi = \text{constant}$, this simplified example is too simple to warrant proclaiming the new method as proven. Nevertheless, this test is well defined and, if the method failed, there would be little point in pursuing it any farther. In the next Section, we put the new algorithm to two rigorous tests.

4. TEST CASES

In this section, we present results of two computations using the MacCormack implicit time-splitting scheme in conjunction with the new algorithm. The full equations of motion are solved for two compressible boundary layers with a full time-averaged Navier-Stokes computer program. The first application is to a Mach 2 laminar boundary layer and the second to a Mach 3 turbulent boundary layer.

4.1 MACH 2 LAMINAR BOUNDARY LAYER

Our first application addresses a Mach 2 flat-plate laminar boundary layer. This case provides a significant test of the new algorithm for two reasons. First, the near-wall ω profile defined in Equation (15) is known to hold through a significant portion of the boundary layer so we have a rigorous check on accuracy. Second, previous computations have often had a nonphysical transition to turbulence even at very low Reynolds numbers.

The finite difference mesh consists of rectangular cells with 12 mesh points in the streamwise direction and 16 points normal to the surface. Mesh points are spaced in a geometric progression with a progression ratio $k = 1.20$. Computation is initiated from uniform flow with the upstream boundary just ahead of the plate leading edge. The downstream boundary lies at a plate-length Reynolds number of $4 \cdot 10^4$. The computation was run for 50 timesteps. Steady flow conditions appear to have been obtained after about 35 timesteps with the quantity χ taking longest of all dependent variables to approach steady state. Computing time for this case is six hours on a TRS-80 microcomputer.

Figure 3 compares a computed ω profile with the theoretical near-wall solution. As indicated, the two solutions are in very close agreement up to about $y^+ = u_\tau y / \nu = 8$. Above this point the near-wall solution is not expected to be valid as convective terms become important. Thus, we can only check our solution in the asymptotic

MACH 2 LAMINAR BOUNDARY LAYER

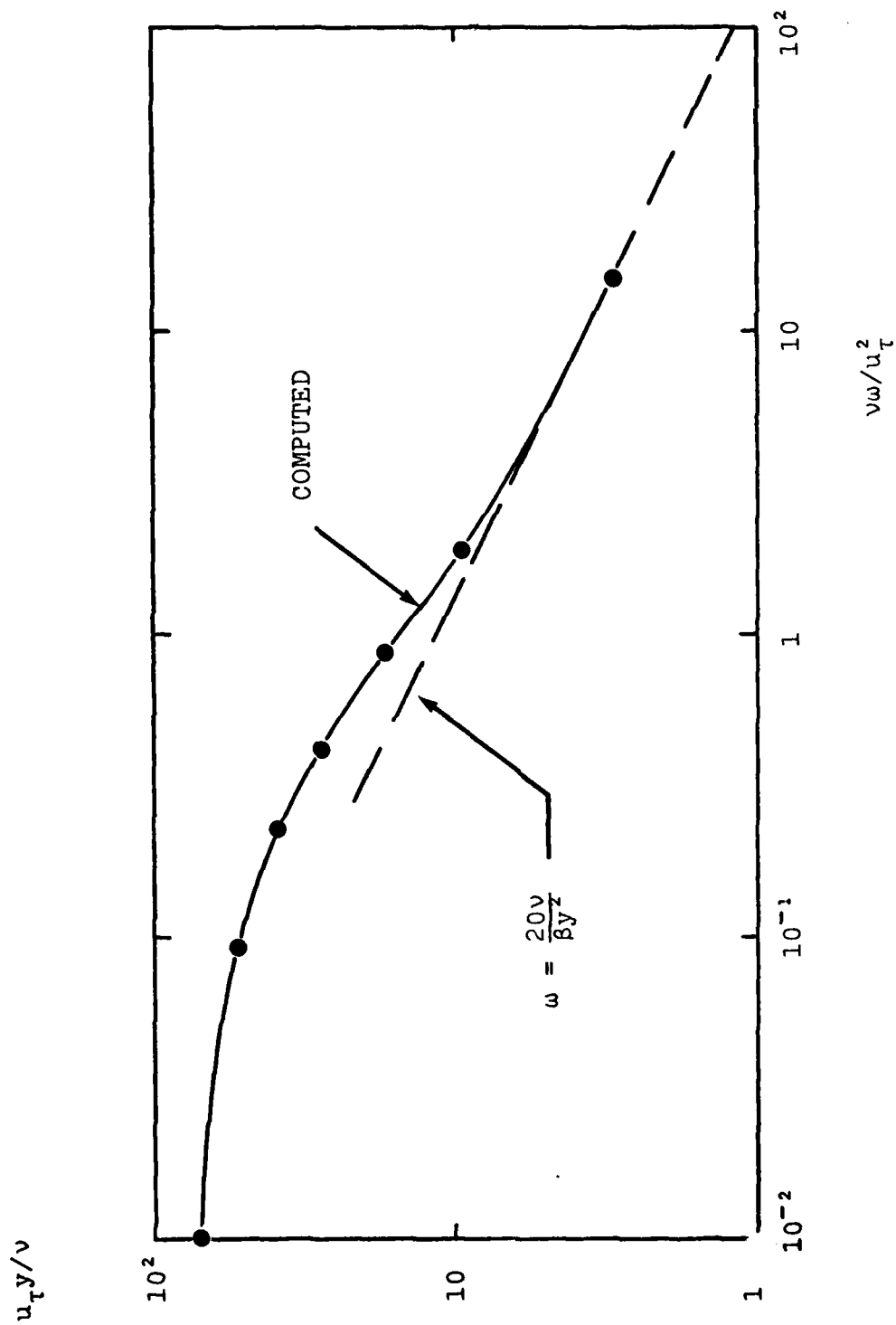


Figure 3. Comparison of computed near-wall dissipation-rate profile with the asymptotic limiting behavior; Mach 2 Laminar boundary layer.

limit $y \rightarrow 0$. However, this is precisely the limit of greatest concern and the overall agreement is excellent.

At no point in the computed flowfield is there any evidence of turbulent energy amplification which might lead to nonphysical transition. The new algorithm thus appears to eliminate this undesired computational result.

Because the boundary layer remains laminar in this computation, the two turbulence model equations play a passive role. To provide an even more rigorous test we must now turn to a case in which the model equations play an active role. In our next application we address such a case.

4.2 MACH 3 TURBULENT BOUNDARY LAYER

In this application we consider a Mach 3 turbulent boundary layer. Again, the mesh consists of 12 points in the streamwise direction and 16 points normal to the surface. The mesh point nearest the surface lies at $y^+ = 2$ and the grid points are placed in a geometric progression with $k = 1.25$. Initial profiles are obtained from a boundary-layer program.

The length of the mesh is 22 boundary-layer thicknesses and Reynolds number based on plate length extends from $1.8 \cdot 10^6$ to $2.5 \cdot 10^6$. The momentum-thickness Reynolds number is 2000 at the upstream boundary.

The main shortcoming of previous Navier-Stokes solutions of the model equations is that, in addition to ω being 20% - 30% too large in the sublayer, skin friction generally is 15% low. Hence, in addition to checking the accuracy of the ω profile, we must also check the skin friction.

Figure 4 compares computed and theoretical ω profiles for the near-wall solution up to $y^+ = 100$. As shown, the numerical solution is within 8% of the theoretical solution below $y^+ = 10$. Between $y^+ = 10$ and 100, the numerical solution asymptotically approaches the wall-layer profile (Equation 16). Thus, ω has been computed far more accurately than in previous Navier-Stokes calculations (cf Figure 1).

MACH 3 TURBULENT BOUNDARY LAYER

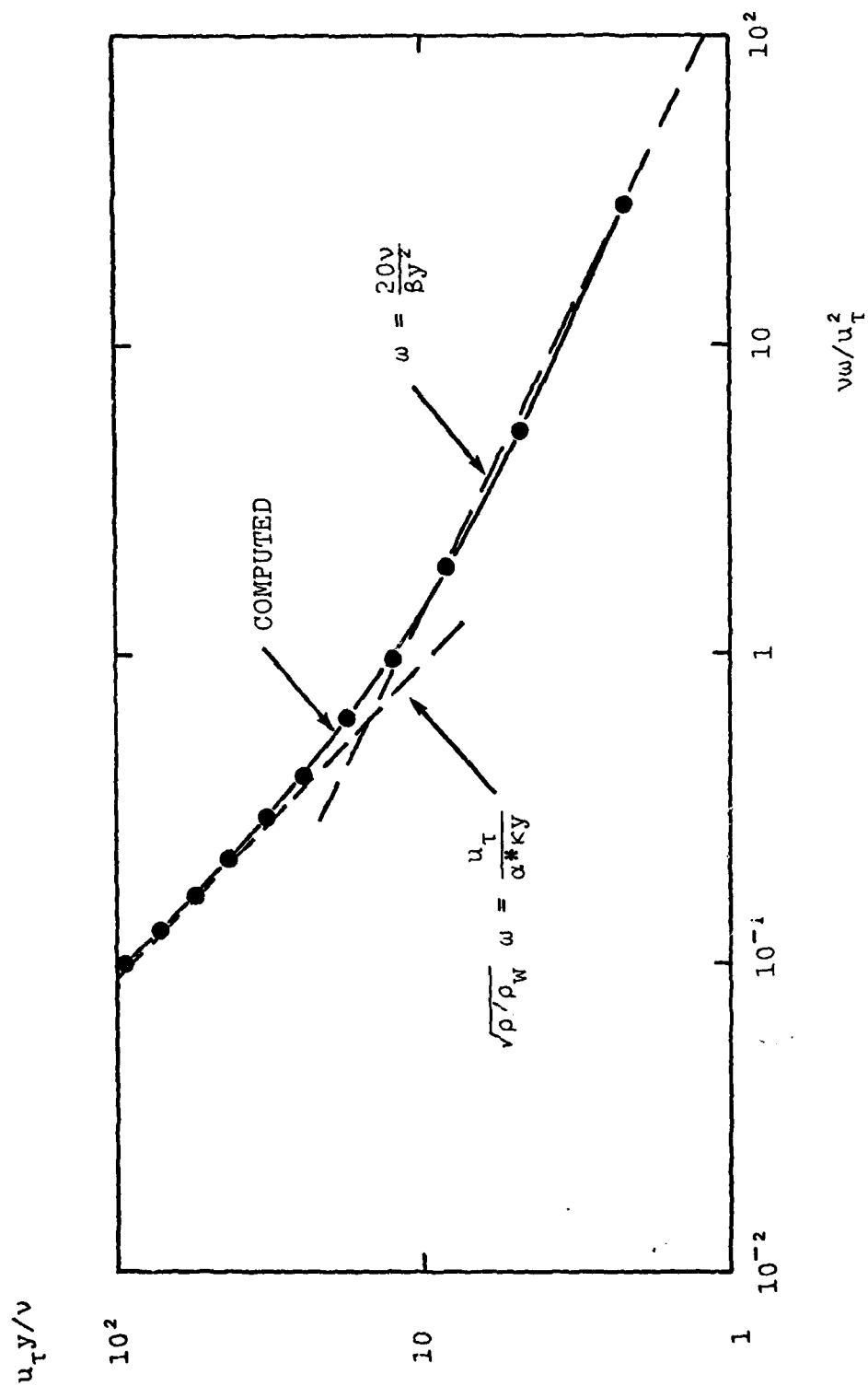


Figure 4. Comparison of computed near-wall dissipation-rate profile with the asymptotic limiting behavior; Mach 3 turbulent boundary layer.

The skin friction coefficient is about 5% lower than in the corresponding boundary-layer computation. This is somewhat surprising as the ω profile is actually underpredicted near the surface. Our earlier arguments would predict a skin friction coefficient which is somewhat overpredicted. The coarseness of the mesh may be responsible. Nevertheless, this application indicates a great improvement in numerical accuracy.

This computation required 125 timesteps to reach steady flow conditions, partly because the timestep was smaller than in the laminar case and partly because χ converged to its steady-state value very slowly. The overall computing time was 15 hours on a TRS-80 microcomputer.

5. RESULTS AND CONCLUSIONS

The new algorithm appears to greatly improve numerical accuracy of a time-marching method when used to compute a quantity such as ω which behaves nonanalytically approaching a solid boundary. This is particularly true when a very crude finite-difference mesh is employed. Although the algorithm has been tested for relatively simple flows, we have no reason to suspect it will fail in more complex applications.

An especially desirable feature of the new algorithm is its independence of the actual numerical method being used. In essence, we have found an analytical method for removing a singularity of varying strength (y^{-4} very close to the surface, y^{-2} farther from the surface). In so doing, the actual equations which are solved numerically can be accurately solved by any conventional method using central differences.

Results presented in Sections 3 and 4 warrant further testing and development of the technique. The most immediate tests should be for more complex flows such as shock induced turbulent boundary-layer separation. More development effort is needed to generalize the transformation defined in Equation (30) for arbitrary geometry. After this testing and development has been done we should be ready to proceed toward our original goal, viz, that of generating accurate numerical solutions for general flow applications such as those occurring in axial turbomachines.

BIBLIOGRAPHY

The period of performance on this Contract was March 1, 1978 to December 31, 1981. During that time the following four Interim Reports describing progress on the Contract were written.

1. Wilcox, D.C., "Development of a Viscous Theory of Three-Dimensional Flow in Highly-Loaded Axial Turbomachines," DCW Industries Report DCW-R-21-01 (June 1979).
2. Wilcox, D.C., "Progress in Developing a Method for Predicting Flow in Axial Turbomachines," DCW Industries Report DCW-R-21-02 (April 1980).
3. Wilcox, D.C., "Progress in Developing a Method for Predicting Flow in Axial Turbomachines," DCW Industries Report DCW-R-21-02A (March 1981).
4. Wilcox, D.C., "Computations With a Two-Equation Model of Turbulence for the 1981 Stanford Olympics," DCW Industries Report DCW-R-21-03 (July 1981).

Additionally, a paper bearing the same title as this Final Report is in preparation for submittal to the AIAA Journal.

CONTRACT OVERVIEW

The overall object of this project has been to develop a method for computing flow through the rotor passages of highly-loaded axial turbomachines. Initially the technical approach was to use the MacCormack hybrid method⁵ to compute the inviscid flow and to use a three-dimensional boundary-layer program to resolve the boundary layers up to separation. As the project progressed, it became evident that coupling the inviscid flow program with the boundary-layer program was proving far more difficult than anticipated because of numerical problems associated with (a) obtaining smooth pressure gradient input for the boundary-layer program and (b) numerically accurate boundary-layer profiles without using inordinate numbers of mesh points normal to blade surfaces. Noting the great promise offered by the new MacCormack implicit method⁶, we decided to eliminate the coupled inviscid/boundary-layer computational procedure in favor of a full time-averaged Navier-Stokes computation.

A sophisticated mesh generation procedure was developed for rotor passages and all program modifications were made to incorporate viscous stresses in the program.

At this point we found that serious truncation error and numerical stability problems were present in the computer program which precluded definitive testing of the method. These problems are delineated in Section 2 of this report. In order to analyze and eliminate these problems, the study reported herein was conducted. Although the algorithm devised in this study has not been incorporated in our turbo-machine program, we have little doubt that it will resolve the difficulties encountered.

An additional task was added to the contract to perform computations for the 1981 Stanford Conference on Complex Turbulent Flows. Results of those computations appear in Reference 4 of the Bibliography.

REFERENCE

1. Wilcox, D.C., "Effects of Streamline Curvature on Turbulent Boundary Layer Separation," DCW Industries Report DCW-R-24-02 (Nov 1980).
2. Wilcox, D.C. and Rubesin, M.W., "Progress in Turbulence Modeling for Complex Flowfields Including Effects of Compressibility," NASA TP-1517 (1979).
3. Favre, A.J., "The Equations of Compressible Turbulent Gases," Annual Summary Report No 1, Institute de Mechanique Statistique de la Turbulence (1965).
4. MacCormack, R.W., "The Effect of Viscosity in Hypervelocity Impact Cratering," AIAA Paper 69-354 (1969).
5. MacCormack, R.W., "An Efficient Numerical Method for Solving the Time Dependent Compressible Navier-Stokes Equations at High Reynolds Number," Computing in Applied Mechanics, AMD Vol 18, ASME (1976).
6. MacCormack, R.W., "A Numerical Method for Solving the Equations of Compressible Viscous Flows," AIAA Paper 81-0110 (1981).
7. Saffman, P.G. and Wilcox, D.C., "Turbulence-Model Predictions for Turbulent Boundary Layers," AIAA Journal, Vol 15, No 4, pp 541-546 (1971).

